Thermoreflectance based thermal microscope

James Christofferson[a] and Ali Shakouri
Jack Baskin School of Engineering, University of California at Santa Cruz, 1156 High Street, Santa Cruz, California 95064

(Received 30 June 2004; accepted 15 November 2004; published online 10 January 2005)

Thermal images of active semiconductor devices are acquired and processed in real time using visible light thermoreflectance imaging with 34 mK sensitivity. By using a 16×16 alternating current coupled photodiode array with synchronous frequency domain filtering a dynamic range of 123 dB is achieved for 1 s averaging. Thus with a stable and higher power light source, fundamentally the camera can reach 6 mK sensitivity over a submicron area. The number of pixels in the image is increased to 160×160 by multiple frame image enhancement and submicron spatial resolution is achieved. The photodiode array system has a maximum 40 kHz frame rate and generates a synchronous trigger for recovery of the phase signal. Amplitude and phase images of the thermoreflectance signal for 50×50 micron square active SiGe based microcoolers are presented. © *2005 American Institute of Physics.* [DOI: 10.1063/1.1850632]

I. INTRODUCTION

The next barrier for developing reliable, small, and fast semiconductor and optoelectronic devices is managing the heat generated in these structures. Temperature measurements on such devices are important, but thermal imaging of micron sized semiconductor devices is nontrival.[1–3] Based on thermoreflectance, a noncontact, all optical, thermal imaging microscope has been built which achieves 34 mK resolution for real time 1 s frames, and 0.34 K resolution at submicron spatial resolution when measuring the temperature of the device metal. The achievable signal to noise ratio (SNR) is limited by the maximum light power per area that is focused on the sample, and noise from the illumination source. Fundamentally, with optimum illumination and considering the total system noise of 100 $fA/Hz^{1/2}$ root-mean-square, the shot noise will limit the thermal sensitivity to 6 mK over a submicron area using a 1 Hz filter. This is an improvement in performance over infrared based systems which are diffraction limited to $3-5$ μm spatial resolution, and in simplicity compared to liquid crystal based thermography, which requires potentially destructive surface preparation. The highest resolution thermal images can be obtained using a nanothermocouple,[4–6] or a near field scanning optical microscopy technique, which have about 50 nm spatial resolution. Both techniques require expensive, complex experimental setups and scanning; a thermal image acquisition can take many hours.

II. THERMOREFLECTANCE MEASUREMENTS

Thermoreflectance measurements exploit the change of a material's reflection coefficient with temperature.[7–9] Typically, the thermoreflectance coefficient C_{th}, which describes the normalized change in the reflection coefficient with temperature, for metals in the visible spectrum, is on the order of 10^{-5} per degree Kelvin. Because of this small magnitude, thermoreflectance images with reasonable spatial resolution and high thermal sensitivity cannot be acquired in a typical off the shelf camera system. To acquire thermoreflectance images a precision, visible light imaging system was designed and built.

Previously, a single element photodiode was used with a lock-in amplifier and a scanning translation stage to acquire thermoreflectance thermal images.[10] A typical scanned image takes over 6 h to acquire because each data point requires 1 s of data to create the necessary 1 Hz bandwidth-limiting filter for noise rejection, and additionally a few seconds for the scanner to move and stabilize. To improve the acquisition time, a photodiode array with synchronous multiple point bandwidth filtering is used as the basis for the thermal imaging microscope. This system exhibits a speedup factor of 256 when compared to a single element scan, and thus thermal images can be realized in several minutes.

III. THERMOREFLECTANCE IMAGING

In general, charge coupled device (CCD) based imaging systems utilize an "integrate and shift" architecture, meaning that each row of pixels within the CCD frame is shifted out as a series of charge packets prior to the analog-to-digital conversion, which adds read noise and limits the dynamic range. Without considering the quantization from the analog to digital converter (ADC), ultimately the dynamic range of a pixel in a CCD is limited by the maximum number electrons in the charge packet that is shifted out. This full well capacity limits most CCDs to 100 dB. Additionally, the integration time for each pixel is generally fixed and only with a careful balance of charge up time and proper light intensity can the full well capacity be utilized to achieve the maximum dynamic range.

Even so, Fournier[11] has acquired thermoreflectance images in a CCD based system. In this experiment, the modulated thermoreflectance thermal signal is down converted to

[a]Electronic mail: jchrist@soe.ucsc.edu

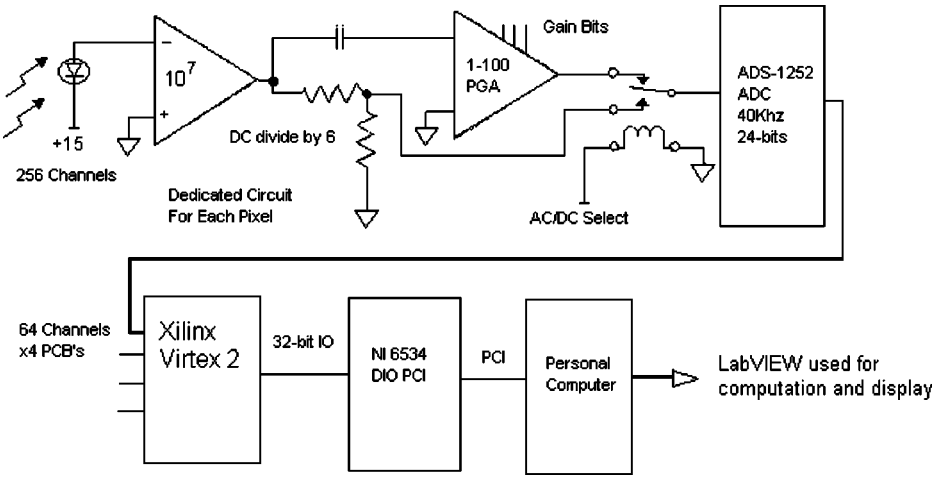

FIG. 1. Single pixel flow of the UCSC thermoreflectance thermal imaging system.

a lower frequency by modulating the illumination source near the thermal cycling frequency. Thus the mixed thermoreflectance thermal image, less than 100 Hz, can be acquired by the slow frame rate of the CCD. Another approach taken by Fournier is to increase the themoreflectance response by optimizing the illumination wavelength to find the maximum thermoreflectance coefficient for the device under test. The thermoreflectance coefficient can vary by an order of magnitude depending on the illumination wavelength and reflection material. Unfortunately, these data are not tabulated and some work is required to find the optimum wavelength for a given material. Fournier achieves good results by applying extensive image processing algorithms and averaging over several minutes. Several degrees Celsius of thermal sensitivity are achieved on the micron scale when applying this imaging technique to microdevices.

In order to be as sensitive as possible, we have developed a non-CCD based thermoreflectance imaging system that can provide potentially higher resolution. The main advantage of a photodiode array based system is the ability to monitor the continuous photocurrent at each pixel, which allows for parallel signal processing. Each pixel is alternating current (ac) coupled in the analog domain and receives additional, programmable gain prior to the analog-to-digital conversion. Thus, the ac component of the signal can be boosted in the analog domain without the direct current (dc) saturation of the pixel. Finally, a dedicated analog to digital converter is provided for each pixel. By using a precision photodiode array with custom electronics instead of a CCD based system, we are creating an imaging system with the highest possible sensitivity.

IV. SYSTEM DESIGN

By piecing together several high performance components, a very high-resolution visible light imaging system has been created. Each pixel has a dedicated circuit depicted in the block diagram, Fig. 1. First, the incident light is acquired by the Hamamatsu C4675 16×16 element photodiode array, which provides a low noise 10^7 transimpedance gain for each pixel. The 256 analog channels are sent to four, in-house designed, printed circuit boards (PCBs); each PCB provides signal conditioning and digitization to 64 channels. The pixel is multiplexed to be ac or dc coupled, and the ac coupled path has an additional 1–100 software selectable gain. All pixels are synchronously sampled by their own Burr–Brown ADS1252 delta sigma ADC at 24 bits and 40 kHz, which is sufficient for recovering signals up to the 16 kHz analog bandwidth of the sensor head. The PCBs then send 256 serial channels to a Xilinx 4M gate Virtex2 FPGA, on a demonstration board from Avnet Design Services. Finally LabVIEW uses direct memory access to read the data via a National Instruments high speed NI-6534 digital input PCI board. Programmed in the Xilinix FPGA is a state machine, which provides the necessary control signals for the ADCs and the serial transfer. A second National Instruments PCI board is used to provide the software-controlled clock, which is buffered and redistributed by the FPGA, the amplifier gain and multiplexer settings, and the control of the streaming data via a RUN/STOP input.

V. REAL TIME THERMAL IMAGES

LabVIEW is used for processing the raw streaming data from the sensor with a fast Fourier transform (FFT) computed on the time domain data of each pixel. This is necessary for limiting the bandwidth of the white noise sources. One advantage to a low pixel count is that up to a frame rate of several kilohertz the data can be processed in less time then the acquisition and the 16×16 pixel thermal images are viewed in real time. At higher frame rates, a 64 Mb buffer is provided to hold several seconds of streaming data. Figure 2 depicts a 1 s frame from the thermal camera when imaging a 50×50 square micron SiGe microcooler[12] shown in the dc image (a). The thermal image (b) of the device is clearly seen when the device is biased at 10 mA. Cooling of 0.25 K below the ambient stage temperature of 297 K is seen on the device, and the cooling extends to the contact layer.

Figure 3 shows the FFT of one pixel of the camera during a thermoreflectance measurement at the spatial resolution of Fig. 2. The peak at 700 Hz is the thermoreflectance signal corresponding to a measurement of 4.4 K above the temperature controlled stage. Also visible are noise harmonics from the light flicker. This spectrum was processed with a 1 s FFT operation with the camera at a maximum 10^9 ac coupled gain. From the peak signal of 130 mV and the noise floor of

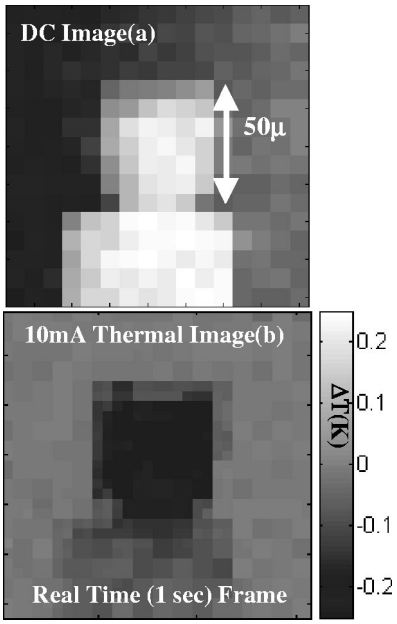

FIG. 2. dc image (a), and thermal image (b) of active 50×50 μm SiGe microcooler. The image was acquired and processed in just over a second.

1 mV the thermal resolution can be calculated to be 34 mK. At a maximum 10^9 ac coupled gain and with the detector covered, the noise floor of the dark current and electronics is 100 fA/Hz$^{1/2}$, while the shot noise of the dc component for Fig. 3 is 474 fA/Hz$^{1/2}$. Considering these values, a total system noise of 484 μV/Hz$^{1/2}$ is obtained, corresponding to 123 dB dynamic range. However, the measurement indicates that the noise floor achieved is about twice this, due to the excess noise in the flicker of the 200 W Hg arc-lamp illumination source. Fundamentally, with more intense and stable illumination, the maximum achievable SNR for a thermoreflectance image in this system can be 6 mK temperature resolution over a submicron area in 1 s.

VI. IMAGE ENHANCEMENT

Because each pixel has an analog output processed with a dedicated ADC, the high performance of the system comes at the drawback of a low pixel count. Thus a scanning technique is used to increase the number of data points in the

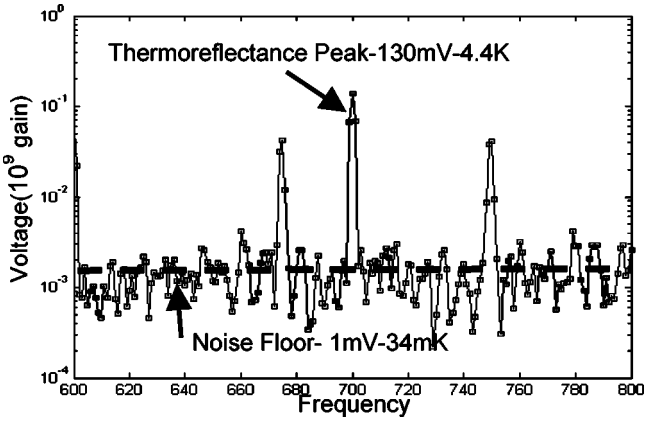

FIG. 3. Fast Fourier transform of one pixel during a 1 s measurement. 34 mK noise floor is achieved.

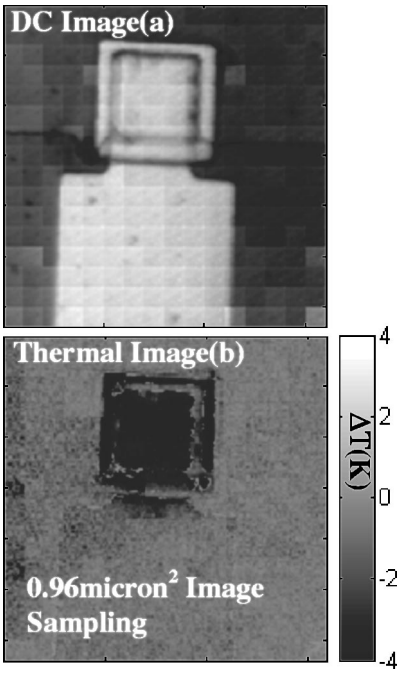

FIG. 4. Enhanced dc image (a) and thermal image (b), of active 50×50 microcooler. At a spatial resolution of 0.96 μm^2 the thermal resolution is reduced.

image. To avoid a long scan range, or complicated image deconvolution, a pinhole array was fabricated and used with the 16×16 array. Two pinhole arrays were fabricated that are 1/25, and 1/100 of the pixel area, thus the thermal image can be improved from a 16×16 low-resolution frame to a higher 80×80, or 160×160 data point frame without any image processing. Due to the variation of the pinhole size, and the tolerances in the integrated circuits used at each pixel, it was necessary to correct the offset, and gain for each pixel, by using software.

Of course, the trade-off for this method is that in reducing the light power, the contribution of the system noise and shot noise is greater. In using the pinhole array the image sampling is improved, but the SNR of the thermal image is decreased. Figure 4 shows a $5\times$ enhancement of the dc image (a), and thermal image (b). The image sampling is 0.96 μm^2. At this small photocurrent, the shot noise, and amplifier noise are on the same order and the noise floor is 100 fA/Hz$^{1/2}$. The SNR scales with the light power down to the amplifier noise, and with only 4% of the total light power per pixel, the thermal resolution for submicron thermal images increases to 0.34 K. The image demonstrates a practical limit, without improving upon the 200 W arc lamp source used for illumination

VII. SYNCHRONOUS SAMPLING AND PHASE IMAGING

The magnitude of the reflected signal obtained with the FFT provides information about the magnitude of the temperature change on the surface, however, to recover the sign of the thermal magnitude requires that the device cycling frequency and the camera frame acquisition are synchronized, allowing for the recovery of the phase signal between

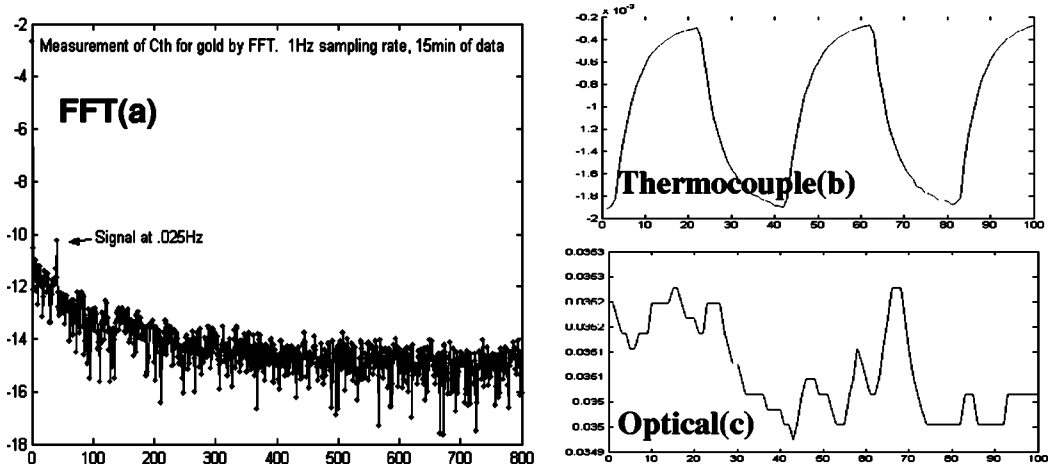

FIG. 5. Determination of thermoreflectance coefficients; the frequency domain thermoreflectance signal (a) at a slow 0.25 Hz acquired over 15 min and time domain signal of 100 s of the measurement showing simultaneous thermocouple (b) and thermoreflectance (c) data.

the excitation and measured result. Because of the synchronized, nonmultiplexed ADCs at each pixel, a single frame maintains the phase between pixels, but without a synchronous trigger, the phase between separate frames would be lost and the image enhancement for the phase as described earlier would not be possible. To allow for enhancement of the phase image beyond 16×16 pixels, synchronous detection is accomplished with a variable frequency trigger that is initiated upon, and synchronized to the frame acquisition. This is entirely controlled with the user software by a programmable timer with a TTL trigger output.

The sign of the magnitude can indicate whether or not the temperatures change from ambient is positive or negative, but it also is modified by the sign of the thermoreflectance coefficient obtained during calibration (Fig. 5). From calibration, it was measured that the substrate material and the metal have a different overall sign of the thermoreflectance coefficient. Figure 6 shows an example of a phase image series of a 50×50 μms SiGe microcooler at increasing bias current. At low currents, 100 mA, the phase image (a) indicates cooling on the device surface (light) and also cooling on the substrate (dark) around the device. Here, the phase change is from sign of the different materials' thermoreflectance coefficient. As the bias current is increased, to 300 (b), 400 (c), and 500 mA (d), the heating on the contact metal (dark) eventually dominates, while the cooling on the metal (light) becomes localized to the device surface. The data on the substrate around the cooler indicate that at 100 mA the substrate is below ambient, but at 400 mA the substrate is above ambient. The phase image series in Fig. 6 shows how the boundary from heating to cooling on the metal changes with bias current. The phase image of the thermoreflectance signal provides important information about the sign of the magnitude, but additionally, phase imaging provides information about propagation of the thermal signal.[13,14]

VIII. CALIBRATION

Unfortunately, thermoreflectance coefficients are not published in the literature, and because of the wavelength and surface texture dependencies, it is necessary to develop a method for external calibration. To this extent, a setup similar to Dilhaire's,[15] involving a microthermocouple, and an external thermoelectric (TE) heater, is used. Dilhaire uses a self-focusing laser beam, required in order to compensate for the high magnification lens and the thermal expansion of the material. Because our setup uses an incoherent broad-spectrum 200 W Hg arc lamp and a microscope objective with a less-sensitive focus, good results were achieved without using this component.

However, even though the small TE heater can heat the sample under test by 20 deg, due to the weak thermoreflectance coefficient, a dc measurement is still too noisy to be resolved. Similar to the previously described method, the measurement bandwidth can be reduced by cycling the temperature of the sample under test many times and processing the result. The thermal transient of an external TE heater is on the order of 30 s, even so, by averaging over 10 min or so, the white noise can be reduced to obtain reasonable signal to noise on the thermoreflectance coefficient. The area of light integration can be increased and thus the overall reflection power is increased (trading spatial resolution for more

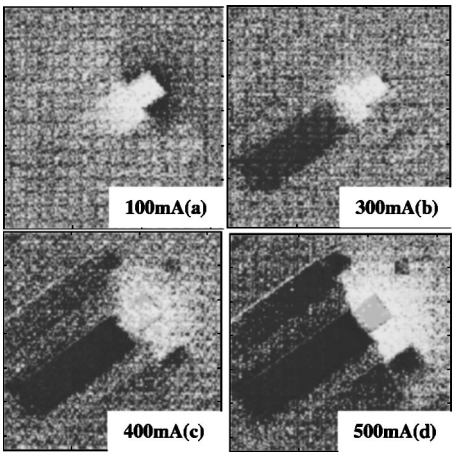

FIG. 6. Phase images of a 50×50 μm SiGe microcooler at increasing bias current. At lower currents, 100 (a) and 300 mA (b), the device cooling extends in to the contact layer while at higher bias, 400 (c) and 500 mA (d), the cooling is localized to the device.

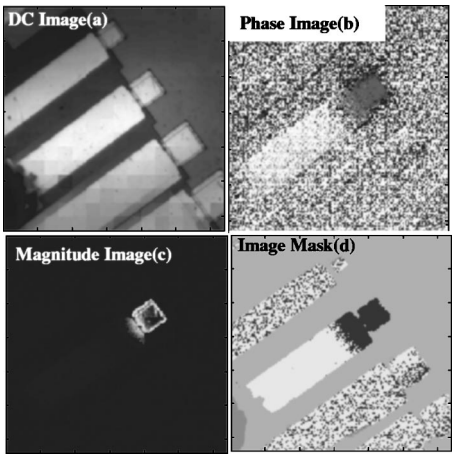

FIG. 7. Data used for realization of thermal image. The dc normalization (a), phase (b), and magnitude (c) images are used to generate a mask (d) to realize the final thermal image.

light power). Simultaneously with the optical measurement, a microthermocouple of 50 μs in diameter is in contact with the material surface under test providing reliable temperature measurement. With this test setup various thermoreflectance coefficients for our white illumination source on different materials can be determined.

In order to use the calibration, the thermal imaging data from the camera head require some basic image processing. The steps toward realizing a thermal image consists of: sign correction, normalization, shadow elimination, and assigning calibration data to different materials in the image. One way to differentiate between different materials in the image, for assigning calibration coefficients is to look at the overall reflectivity of the different surfaces in the image histogram. Generally, the metal surface corresponds to the bright points in the image, while the dark points are the substrate material. From this bimodal image histogram, the shadow points are removed, and coefficients are assigned to the different surfaces.

In a similar way, the histogram of the phase image can give information about the data points corresponding to the sign of the temperature change in the image. This information is used to generate an image mask, which is then multiplied with the data. Figure 7 shows the acquired dc image (a), phase image (b), magnitude image (c), and the generated image mask (d).

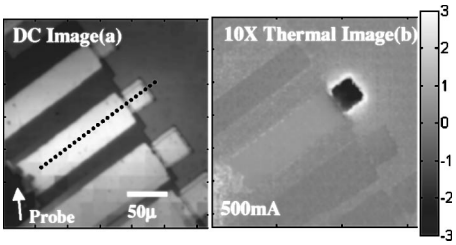

FIG. 8. Typical results: dc image (a) and thermal image (b) acquired on a 50×50 μm SiGe microcooler biased at 500 mA, 30 C stage temperature. This device is limited by heating on the substrate, probably due to too much resistance between the superlattice and buffer layer. The dotted line is the cross section used in the following figure.

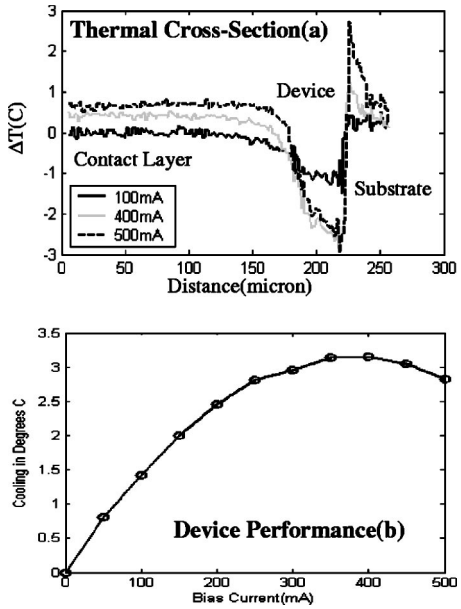

FIG. 9. Quantitative analysis: Average surface temperature (a) and cross sections (b) of active 50×50 μm microcooler. Ten images of the microcooler at increasing bias current show a maximum surface cooling of 3.2 from 30 C stage temperature. Cross sections down the contact layer to the microcooling surface shows good cooling distribution on the device but too much heating on the substrate around the device.

IX. EXPERIMENTAL RESULTS

Presented are typical results of an active 50×50 μm square SiGe microcooler. Figure 8 shows the microcooler device (a) and the $10\times$ enhanced thermal image (b) of the device when biased to 500 mA. The thermal image indicates that the device cools 2.8 C below the 30 C stage on the device surface at 500 mA, but additionally, there is heating on the substrate around the device. Simulations indicate that there should not be as much heating occurring on the substrate around the device. The extra heating is probably caused by too much resistance in the buffer layer of the microcooler structure. Figure 9 depicts quantitative analysis of the thermal images, the device surface cooling as a function of bias current (a) and thermal cross sections down the contact layer to the device (b). Such data are important for providing feedback to the design engineers to minimize parasitic heat sources. This shows that the thermoreflectance array camera is an important tool in the investigation of microscale thermal phenomena, and represents an improvement over commercially available thermal microscopes.

ACKNOWLEDGMENTS

Thanks to Chris Labounty, Gehong Zeng, Xiaofeng Fan, John Bowers of UC Santa Barbara and Edward Croke of HRL laboratories for the microdevice fabrication. This work was funded by Packard Foundation.

[1] J. Kolzer, E. Oesterschulze, and G. Deboy, Microelectron. Eng. **31**, 251 (1996).
[2] A. Cutolo, Rev. Sci. Instrum. **69**, 337 (1998).
[3] J. Altet *et al.*, Microelectron. J. **33**, 689 (2002).
[4] A. Majumdar, K. Luo, Z. Shi, and J. Varesi, Exp. Heat Transfer **8**, 83 (1996).
[5] J.-H. Lee and Y. B. Gianchandani, Rev. Sci. Instrum. **75**, 1222 (2004).

[6] M.-H. Li and Y. B. Gianchandani, J. Vac. Sci. Technol. B **18**, 3600 (2000).
[7] Y. S. Ju and K. E. Goodson, J. Heat Transfer **120**, 306 (1998).
[8] V. Quintard, S. Dilhaire, P. Tam, and W. Claeys, IEEE Trans. Instrum. Meas. **48**, 69 (1999).
[9] A. M. Mansanares, D. Fournier, and A. C. Boccara, Electron. Lett. **29**, 2045 (1993).
[10] J. Christofferson, D. Vashaee, A. Shakouri, and P. Melese, *Proceedings of the International Mechanical Engineering Congress and Exhibition*, New York, 2001.
[11] S. Grauby, B. C. Forget, S. Hole, and D. Fournier, Rev. Sci. Instrum. **70**, 3603 (1999).
[12] G. Zeng *et al.*, Electron. Lett. **35**, 2146 (1999).
[13] A. Rosencwaig, J. Opsal, W. L. Smith, and D. L. Willenborg, Appl. Phys. Lett. **46**, 1013 (1985).
[14] D. Fournier, MRS Bull. **26**, 465 (2001).
[15] S. Dilhaire, S. Jorez, L. D. Patino Lopez, and W. Claeys, *Proceedings of the International Conference on Photoacoustic and Photothermal Phenomena*, Kyoto, Japan, 2000.